RSC Advances

PAPER

View Article Online
View Journal | View Issue

Cite this: *RSC Adv.*, 2025, **15**, 25620

Bio-inspired benzimidazole-functionalized manganese terpyridine complexes for electrochemical CO_2 reduction†

Runqi Mo, Rui Li, Ping Zhang, Ying Xiong and Lin Chen *

Inspired by the active site of carbon monoxide dehydrogenase (CODH), where a pair of amino acids facilitating hydrogen bonding manages the reversible interconversion of CO and CO_2 with high efficiency, we developed a family of manganese terpyridine derivatives (**1–4**), in which a benzimidazole moiety functions as a proton relay to assist the CO_2 reduction reaction (CO_2RR). To regulate the position of the proton donor, the benzimidazole moiety was introduced into the framework by two approaches, and the pK_a of the proton relay was adjusted by methylation of the benzimidazole moiety. We found that all such designs led to a sharp corruption in the activity of electrochemical CO_2 reduction compared with that of our previously reported analogues. The corruption was ascribed to the pK_a of the benzimidazole moiety, which resulted in inefficient proton exchange.

Received 6th March 2025
Accepted 20th June 2025

DOI: 10.1039/d5ra01621e

rsc.li/rsc-advances

Introduction

In the past decade, extensive efforts have been devoted for exploring highly efficient catalysts for the CO_2 reduction reaction (CO_2RR).[1] Owing to their rich electronic and structural tunability, transition-metal-based molecules have been utilized to systematically investigate CO_2RR mechanisms.[2] Mononuclear metal complexes, such as chromium,[3] manganese,[4–9] iron,[10–12] cobalt,[13] nickel,[14] ruthenium,[15] and rhenium,[16,17] have exhibited activity in the electrochemical CO_2RR. In the [NiFe] carbon monoxide dehydrogenase (CODH) active site (Scheme 1),[18] a redox active nickel center, an iron(II) ion acting as a Lewis acid, and a pair of amino acids facilitating hydrogen bonding manage the reversible interconversion of CO and CO_2 with high efficiency. The second-sphere histidine and lysine residues in Ni–Fe CODH are positioned to stabilize the CO_2–metal adduct and assist in the C–O bond cleavage.[18] Inspired by the active site of CODH, installing a proton relay inside the second coordination sphere of catalysts has proven to be instrumental in improving the catalysis of the CO_2RR.[9,19–21] Previously, we systematically investigated a series of manganese terpyridine complexes (**M1**–**M4**) bearing a proximal proton relay (Scheme 1). **M1** exhibits significantly higher selectivity than its bipyridine analogues.[22] Both catalysts (**M2** and **M3**) exhibit high selectivity for CO_2-to-CO conversion, and the isomer with a proximal amide (**M3**) shows a rate *ca.* two orders of magnitude higher than that of the isomer with a distal amide.[23] Furthermore, Mn terpyridine derivatives with urea groups (**M4**) functioning as multipoint hydrogen-bonding hangman accelerate the reaction rate of CO_2 reduction to *ca.* 360 s^{-1}.[24] These studies confirm the key influence of a proximal proton relay in improving the CO_2RR. However, much improvement is still

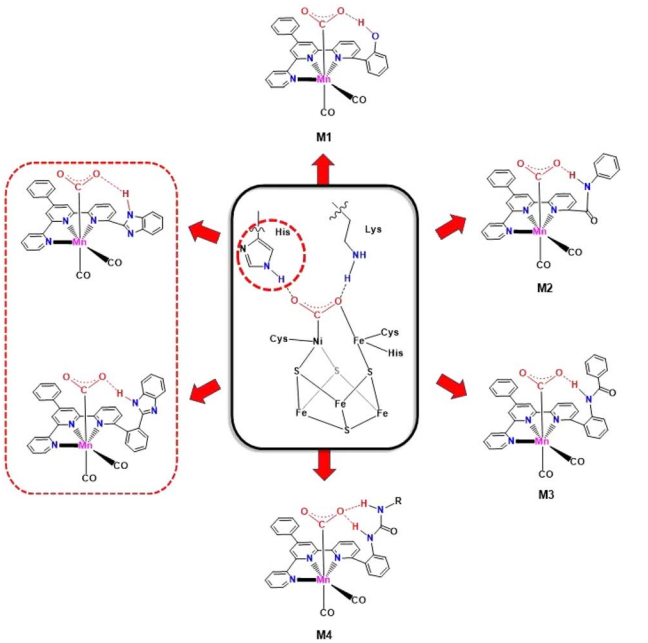

Scheme 1 Active site of Ni–Fe CO dehydrogenase inspires the design of a series of manganese terpyridine dicarbonyl catalytic active sites. The catalytic active sites in the red dashed box are studied in this work.

State Key Laboratory of Environment-Friendly Energy Material, School of Materials and Chemistry, Southwest University of Science and Technology, Mianyang 621010, P. R. China. E-mail: chenlin101101@aliyun.com

† Electronic supplementary information (ESI) available. See DOI: https://doi.org/10.1039/d5ra01621e

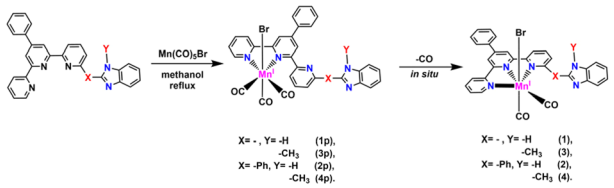

Scheme 2 Preparation of manganese catalysts **1–4**.

needed to optimize the synergism between the proton relay and the Mn terpyridine framework.

To better mimic to the structure of the natural enzyme CODH, in this study, a benzimidazole moiety was introduced into the second coordination sphere of the Mn terpyridine framework to assist the CO_2RR (Scheme 1, the red dashed box). As shown in Scheme 2, the benzimidazole moiety was incorporated into the framework by two approaches. One approach involves attaching the benzimidazole moiety to the pyridine without a spacer, and the other involves separating the benzimidazole moiety and pyridine with a phenyl spacer. The distance between the proton donor and CO_2 adduct could be adjusted by rotating the benzimidazole moiety or phenyl (Scheme S10†). In addition, the benzimidazole moiety was methylated to regulate the pK_a of the proton relay. Herein, the electrochemical reduction of CO_2 using this series of complexes was studied.

Results and discussion

Synthesis and characterization

Precursors **1p–4p** were obtained according to our previously reported methods (Schemes 2 and S1–S8†) by refluxing $Mn(CO)_5Br$ and the corresponding ligands L1–L4 in methanol, respectively.[25] All of the complexes were characterized by high-resolution mass spectroscopic (HR-MS), ^{1}H NMR, FTIR and elemental analyses (Fig. S1–S13†). The configurations of **1p–4p** are hypothesized to resemble those of the analogues reported previously,[23] in which the terpyridine serves as a bidentate ligand, the pyridyl proximal to the benzimidazole moiety is uncoordinated (Scheme 2), and bromide is located at an apex, opposite the axial carbonyl. IR and HR-MS indicate that the Mn(I) centre of these complexes is coordinated with three CO ligands in a facial mode.[7] The ^{1}H NMR spectroscopy of these complexes indicates a mixture of atropisomers (the NH or N–CH_3 moieties parallel and antiparallel to the axial plane).[21]

In situ conversion of the coordination mode from k^2-*N*,*N*′,*N*″-tpy (k^2-tpy) to k^3-*N*,*N*′,*N*″-tpy (k^3-tpy)

As reported in our previous studies,[22,23] the target catalysts **1–4** can be *in situ* obtained decarbonylating of precursors **1p–4p** promoted by an electric field (*ca.* −1.5 V *vs.* $Fc^{+/0}$). The switch in the coordination mode is very complicated. As reported by Kubiak *et al.*, the k^2-mode reductive intermediates *in situ* transform to the corresponding k^3 mode.[7] Our previous studies found that the switch in the coordination mode always occurs before the reduction reaction.[22–25] In this study, the switch process was monitored by infrared spectroelectrochemistry (IR-SEC) performed in a self-designed thin-layer specular reflectance cell under Ar.

As shown in Fig. S14–S17† (red line), precursors **1p–4p** studied herein almost inherit the features reported previously and *in situ* convert to k^3-mode complexes **1–4** (IR absorption at around 1949, 1925, 1878 and 1853 cm^{-1}) with the help of an electric field before the reduction reaction. Subsequently, at a more negative applied potential, the reduction of **1p–4p** results in a mixture of [X^{2-}–Br^-] and [Xp^{2-}–Br^-] (X = **1–4**). Herein, [X^{2-}–Br^-] may be obtained from the reduction of X or decarbonylating of [Xp^{2-}–Br^-]. Observably, [Xp^{2-}–Br^-] cannot totally convert to [X^{2-}–Br^-] in the timescale of the IR scan. Among all these complexes, **2p** possesses the largest ratio of [X^{2-}–Br^-]/[Xp^{2-}–Br^-] in the intensity of IR absorption, indicating the higher stability of [2^{2-}–Br^-] compared to the other [X^{2-}–Br^-]. In addition, the two lower-intensity absorption bands at around 1983 and 1892 cm^{-1} for **1p** and **3p** are assigned to the [Mn^0-bipyridine]$_2$ dimer[22] (Fig. S14 and S16†), while the IR signal at 1983 and 1892 cm^{-1} cannot be found for **2p** and **4p** with a phenyl linkage (Fig. S15 and S17†), indicating that the bulky ligand eliminates this dimerization.

Electrochemical properties

The cyclic voltammograms (CVs) of all complexes were tested in CH_3CN (all potentials are reported against ferrocene, $Fc^{+/0}$, *ca.* 0.63 V *vs.* NHE). As shown in Fig. 1a, complex **1p** features two successive irreversible reduction peaks at around −1.5 V and one reversible couple at −2.0 V. The former can be assigned to the successive reduction on the Mn center and the ligand.[7] The latter is ascribed to the redox of the intermediate formed by

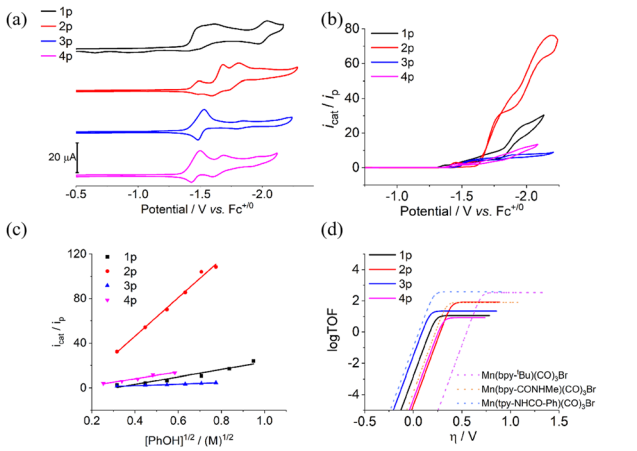

Fig. 1 Cyclic voltammograms of 0.5 mM complexes **1p–4p** (a) under Ar and (b) under CO_2 in the presence of 1 M phenol. (c) Dependence of the catalytic current (i_{cat}) on the square root of the concentration of phenol. (d) Catalytic Tafel plots of CO_2-to-CO conversion showing the relationship between the TOF and driving force (using foot-of-the-wave analysis), compared to previously reported electrocatalysts Mn(bpy-^{t}Bu)(CO)$_3$Br, Mn(bpy-CONHMe)(CO)$_3$Br, and Mn(tpy-NHCO-Ph)(CO)$_3$Br. Scan rate = 100 mV s^{-1}, 0.1 M ^{n}Bu$_4$NPF$_6$ in CH_3CN, glassy carbon working electrode, Ag^+/Ag reference electrode, and Pt wire counter electrode.

intramolecular proton transfer from the benzimidazole to reductive Mn center following the two successive reduction events.[9,21,22] The intramolecular proton transfer leads to the irreversibility of the former reduction events. By contrast, the methylation of benzimidazole results in the reversible redox couple for complex **3p** and the lack of the Mn–H intermediate.[9,21,22] The difference between complexes **2p** and **4p** lies in the methylation on the benzimidazole moiety. The difference exhibits negligible influence on the initial states of **2p** and **4p** as well as the k^3 modes **2** and **4** (Fig. S18†). The significant contrast between CVs of **2p** and **4p** may be ascribed to the intramolecular electron transfer following the double reduction of **2**. The reduction waves, consistent with those of **4**, are assigned to the successive reduction of **2**, and the third new peak is assigned to reduction on the *in situ*-formed Mn hydride. This difference soundly supports the transformation in the coordination modes for **2p** and **4p** before the reduction because the k^3 mode shortens the proton transfer distance between the proton donor and reductive Mn center. In addition, the Mn hydride is responsible for the strong response to phenol with **2p**, which is discussed in the next section.

The differential pulse voltammogram (DPV) tests of **1p–4p** are consistent with the reduction events in CVs (Fig. S14–S17†). Furthermore, the cathodic and anodic peak currents (i_p) of complexes **1p–4p** show linear correlations with the square root of the scan rate ($v^{1/2}$) from 0.025 to 10 V s^{-1} under Ar (Fig. S19–S22†), consistent with diffusion-controlled processes described by the Randles–Sevcik equation.[13] The electrochemical property parameters of complexes **1p–4p** are summarized in Table 1.

After the addition of phenol, **1p–4p** exhibit different responses to protons. The response to protons follows the order of **2p** >> **1p** > **3p** >> **4p** (Fig. S23–S26†). As shown in Fig. S23,† **1p** catalyzes the proton reduction to hydrogen at −2.0 V, which is based on the redox couple of the Mn–H hydride. The third reversible redox event for complex **2p** matches well with the reduction of phenol, leading to a strong increase in the current as the concentration of phenol. Complex **3p** mediates the conversion of the proton to hydrogen with an obviously lower overpotential, but the amplitude of the catalytic current is low. Complex **4p** exhibits a weak response to phenol following the second reduction peak. According to our previous studies, in the *in situ*-formed k^3 mode, the benzimidazole moiety in **2** features the best position and pK_a to assist the proton transfer to the Mn center. The configuration and performance of **2** are very similar to those of our previously reported analogue with a carboxylic acid proton relay.[25] By contrast, the distance between the proton relay and Mn center in complex **3** is significantly longer than that in complex **2**.[22]

After saturating the test solution with CO_2 in the presence of 1 M phenol, complexes **1p–4p** exhibit varied responses (i_{cat}/i_p) to CO_2. Among these complexes, **2p** exhibits the strongest response to CO_2 (Fig. 1b). As shown in Fig. S24,† CO_2 leads to a sharp increase in the current at *ca.* 100 mV, more positive than that for proton reduction, corresponding to the reduction of CO_2 to CO. The catalytic wave of complex **2p** can be divided into two sections at the catalytic current plateau (Fig. 1b). The first section is assigned to the CO_2 reduction, while the other section is ascribed to the reduction of protons, similar to that in the absence of CO_2 (Fig. S24†). The catalytic half-wave potential for **2p** is *ca.* −1.75 V, corresponding to an overpotential of *ca.* 400 mV ($E^{\theta}_{CO_2/CO} = -1.35$ V *vs.* $Fc^{+/0}$).[10] By contrast, complexes **3p** and **4p** feature lower overpotentials (*ca.* 250 mV), while the catalytic current becomes observably lower. The catalytic activity for CO_2 reduction of complex **1p** is a little stronger than that of **3p** and **4p**.

To be consistent with the previous Mn polypyridine analogues, external phenol is essential for the CO_2-to-CO conversion using **1p–4p**.[16] As shown in Fig. 1c, the i_{cat}/i_p values of **1p–4p** show a linear dependence on the square root of the concentration of phenol, indicating a first-order dependence on the concentration (Fig. 1c and S27–S30†).[26] Kinetic studies found the current response (i_{cat}/i_p) of complexes **1p–4p** all exhibit linear dependence on the catalyst concentration (Fig. S31–S34†). Among these complexes, **2p** is the most sensitive to the concentrations of the catalyst and phenol. However, as the scan rate increases (Fig. S35–S38†), the conversion in the coordination mode (k^2 to k^3) cannot keep pace with the electrochemical reduction reaction; therefore, the catalytic contribution of the k^2 mode increases at a higher scan rate.[23]

To compare the CO_2 reduction activity of **1p–4p** and other catalysts, the TOF_{max} values of **1p–4p** were calculated by foot-of-the-wave analysis (FOWA) (Fig. 1d and S39†)[26] under general conditions (in the presence of 1 M phenol, under CO_2 saturation, and at a scan rate of 100 mV s^{-1}), and the plateau current of the first section was adopted for the calculation. The state-of-the-art benchmarking of performances clearly revealed that these new Mn catalysts exhibit worse performances than the previous analogues in terms of the overpotential and catalytic rate (Fig. 1d). The corruption is ascribed to the pK_a of the benzimidazole moiety, which results in the inefficiency of the proton exchange. The acidity of the benzimidazole is stronger than that of amide and urea moieties, which is favorable for the

Table 1 Electrochemical studies of **1p–4p**

Catalyst	E^{θ}_{cat} (V)	η^a (V)	$i_{cat}/i_p{}^b$	$TOF_{CV}{}^c$ (s^{-1})	TON_{CPE}	FE_{total} (%)	$FE_{CO}{}^d$ (%)
1p	−1.58	0.28	8.47	11.31	0.05	97.8% ± 5%	80.8% ± 5%
2p	−1.74	0.39	17.72	81.25	4.50	100.2% ± 5%	61.1% ± 5%
3p	−1.55	0.24	5.67	22.44	4.75	99.2% ± 5%	62.3% ± 5%
4p	−1.66	0.31	4.11	8.48	0.86	99.0% ± 5%	77.3% ± 5%

[a] Derived from catalytic half-wave potentials $\eta = E^{\theta}_{CO_2/CO} - E_{half}$. [b] Obtained at *ca.* −1.80 V. [c] Derived using the equations reported in the ESI file. [d] FE for CO is reported as an average of three CPE experiments at −1.85 V.

transfer of protons from the proton relay to CO_2 adduct but is adverse for regaining protons from the bulk solution. The passable performance of the benzimidazole moiety in the artificial catalyst compared to that in CODH is ascribed to the alkalinity of the catalytic center as well as the CO_2 adduct.

Controlled potential electrolysis (CPE) experiments (Fig. S40†) of all complexes in a CO_2 atmosphere in the presence of 1.0 M phenol at varied potentials were carried out in a custom-designed cell (Fig. S41†). An average current of around 0.5 mA cm^{-2} is observed throughout the electrolysis period of 1 h under an applied potential of −1.85 V. CVs after electrolysis show a slight decrease in the amplitude of the catalytic current (Fig. S42–S44†), consistent with the observation of a decrease in the catalytic current during CPE. The formation of catalytically active nanoparticles is excluded owing to the negligible current observed after a "rinse test" following CPE (Fig. S45†). Therefore, the current decay is ascribed to the decomposition of the catalyst. The analysis of the gas mixture in the headspace of the working compartment by gas chromatography (GC) confirms CO and H_2 as the main products. The analysis of the liquid phase by ion chromatography (IC) detects amounts of formic acid for complexes **1p–4p**. Control experiments show significantly lower current densities and a negligible amount of CO (or H_2 and formic acid) in the absence of catalysts (Fig. S40†). Isotope labelling experiments using $^{13}CO_2$ confirm that CO is formed *via* the reduction of CO_2 (Fig. S46†). The electrocatalytic properties of **1p–4p** are summarized in Tables 1 and S1.† Using product analysis under varied electrolysis potentials, we found that the selectivity of products becomes corrupted as the potential decreases, which is consistent with the observations in CVs. At a more negative scan potential, the contribution of proton reduction becomes strong.

Conclusions

Inspired by the active site of carbon monoxide dehydrogenase (CODH), we integrate the benzimidazole moiety into the manganese terpyridine frame as a proton relay by two approaches. It is a pity that the performance of the benzimidazole moiety in the manganese terpyridine catalyst for the electrochemical CO_2RR is worse than that in CODH. The poor activity of this series of catalysts is because the benzimidazole moiety disrupts the acid–base equilibrium between the proton relay and bulk solution as well as the metal center, reducing the proton exchange speed between the bulk solution and metal center. The results here clearly advise that ongoing studies in the design of CO_2RR catalysts should pay more attention to the balance among the functional fragments of catalysts rather than solely focusing on the resemblance to the structure of natural enzymes. The consideration of the findings presented here in future catalyst designs may lead to more-efficient catalysts.

Data availability

All data supporting this study, including experimental procedures, spectroscopic analyses, ^{1}H-NMR data and electro chemical details, are available within the article and its ESI.†

Author contributions

L. C. designed the research. R. Q. M., R. L., P. Z. performed electrochemistry, synthesis, and analyzed the data. Y. X. and L. C. wrote the manuscript.

Conflicts of interest

There are no conflicts to declare.

Acknowledgements

This research was supported by the Chinese National Natural Science Foundation (U20A20125, 22088102, 22172018 and 21403132), the State Key Laboratory of Environment-Friendly Energy Materials Research on Independent Subjects (20fksy15, 21fksy18), and the State Key Laboratory of Fine Chemicals, Dalian University of Technology (KF2214).

Notes and references

1 K. E. Dalle, J. Warnan, J. J. Leung, B. Reuillard, I. S. Karmel and E. Reisner, *Chem. Rev.*, 2019, **119**, 2752–2875.
2 N. Elgrishi, M. B. Chambers, X. Wang and M. Fontecave, *Chem. Soc. Rev.*, 2017, **46**, 761–796.
3 S. L. Hooe, J. M. Dressel, D. A. Dickie and C. W. Machan, *ACS Catal.*, 2020, **10**, 1146–1151.
4 M. Bourrez, F. Molton, S. Chardon-Noblat and A. Deronzier, *Angew. Chem., Int. Ed.*, 2011, **50**, 9903–9906.
5 J. A. Barrett, C. J. Miller and C. P. Kubiak, *Trends Chem.*, 2021, **3**, 176–187.
6 M. L. Clark, P. L. Cheung, M. Lessio, E. A. Carter and C. P. Kubiak, *ACS Catal.*, 2018, **8**, 2021–2029.
7 C. W. Machan and C. P. Kubiak, *Dalton Trans.*, 2016, **45**, 17179–17186.
8 M. D. Sampson, A. D. Nguyen, K. A. Grice, C. E. Moore, A. L. Rheingold and C. P. Kubiak, *J. Am. Chem. Soc.*, 2014, **136**, 5460–5471.
9 M. H. Rønne, D. Cho, M. R. Madsen, J. B. Jakobsen, S. Eom, É. Escoudé, H. C. D. Hammershøj, D. U. Nielsen, S. U. Pedersen, M.-H. Baik, T. Skrydstrup and K. Daasbjerg, *J. Am. Chem. Soc.*, 2020, **142**, 4265–4275.
10 C. Costentin, S. Drouet, M. Robert and J. M. Saveant, *Science*, 2012, **338**, 90–94.
11 E. M. Nichols, J. S. Derrick, S. K. Nistanaki, P. T. Smith and C. J. Chang, *Chem. Sci.*, 2018, **9**, 2952–2960.
12 P. Gotico, B. Boitrel, R. Guillot, M. Sircoglou, A. Quaranta, Z. Halime, W. Leibl and A. Aukauloo, *Angew. Chem., Int. Ed.*, 2019, **58**, 4504–4509.
13 S. Roy, B. Sharma, J. Pecaut, P. Simon, M. Fontecave, P. D. Tran, E. Derat and V. Artero, *J. Am. Chem. Soc.*, 2017, **139**, 3685–3696.
14 D. Hong, T. Kawanishi, Y. Tsukakoshi, H. Kotani, T. Ishizuka and T. Kojima, *J. Am. Chem. Soc.*, 2019, **141**, 20309–20317.
15 B. A. Johnson, S. Maji, H. Agarwala, T. A. White, E. Mijangos and S. Ott, *Angew. Chem., Int. Ed.*, 2016, **55**, 1825–1829.

16 C. Riplinger, M. D. Sampson, A. M. Ritzmann, C. P. Kubiak and E. A. Carter, *J. Am. Chem. Soc.*, 2014, **136**, 16285–16298.
17 J. M. Smieja, E. E. Benson, B. Kumar, K. A. Grice, C. S. Seu, A. J. M. Miller, J. M. Mayer and C. P. Kubiak, *Proc. Natl. Acad. Sci. U. S. A.*, 2012, **109**, 15646–15650.
18 J. H. Jeoung and H. Dobbek, *Science*, 2007, **318**, 1461–1464.
19 J. B. Jakobsen, M. H. Rønne, K. Daasbjerg and T. Skrydstrup, *Angew. Chem., Int. Ed.*, 2021, **60**, 9174–9179.
20 J. M. Saveant, *Angew. Chem., Int. Ed.*, 2019, **58**, 2125–2128.
21 J. Agarwal, T. W. Shaw, H. F. Schaefer and A. B. Bocarsly, *Inorg. Chem.*, 2015, **54**, 5285–5294.
22 S. He, Y. Qing, P. Zhang, Y. Xiong, Q. Wu, Y. Zhang, L. Chen, F. Huang and F. Li, *Angew. Chem., Int. Ed.*, 2023, **62**, e202216082.
23 Y. Qing, Q. Wu, S. He, P. Zhang, Y. Xiong, Y. Zhang, F. Huang, F. Li and L. Chen, *Dalton Trans.*, 2023, **52**, 14309–14313.
24 M. Li, F. Huang, P. Zhang, Y. Xiong, Y. Zhang, F. Li and L. Chen, *Chem.–Eur. J.*, 2024, **30**, e202304218.
25 Q. Wu, M. Li, S. He, Y. Xiong, P. Zhang, H. Huang, L. Chen, F. Huang and F. Li, *Chem. Commun.*, 2022, **58**, 5128–5131.
26 K. J. Lee, N. Elgrishi, B. Kandemir and J. L. Dempsey, *Nat. Rev. Chem.*, 2017, **1**, 0039.